# Ambient-pressure high-$T_c$ superconductivity in doped boron-nitrogen clathrates La(BN)$_5$ and Y(BN)$_5$

Han-Bin Ding,[1,2] Yu-Jie Feng,[1,2] Meng-Jing Jiang,[1] Hui-Li Tian,[1] Guo-Hua Zhong,[1,3,*] Chun-Lei Yang,[1,3,†] Xiao-Jia Chen,[4,5,‡] and Hai-Qing Lin[6,7]

[1]*Shenzhen Institute of Advanced Technology, Chinese Academy of Sciences, Shenzhen 518055, China*
[2]*Nano Science and Technology Institute, University of Science and Technology of China, Suzhou 215123, China*
[3]*University of Chinese Academy of Sciences, Beijing 100049, China*
[4]*School of Science, Harbin Institute of Technology, Shenzhen 518055, China*
[5]*Center for High Pressure Science and Technology Advanced Research, Shanghai 201203, China*
[6]*School of Physics, Zhejiang University, Hangzhou 310027, China*
[7]*Beijing Computational Science Research Center, Beijing 100193, China*

HPSTAR 1538-2022

(Received 27 June 2022; revised 1 August 2022; accepted 1 September 2022; published 12 September 2022)

$LaH_{10}$ exhibits the near-room-temperature superconductivity, but the high fabrication pressure exceeding 200 GPa limits the possibility of its experimental research and application. To examine the feasibility of high-temperature superconductivity at ambient pressure in light-element compounds, we study the crystal structure, metallization, and electron-phonon interaction of $M(BN)_5$ ($M$ = La and Y) with $LaH_{10}$-like clathrate configuration, based on the first-principles calculations. The result shows that adopting B and N to substitute H, the strong $sp^3$ hybridization between B and N greatly reduces the pressure to keep the dynamical stability. We predict that the strong electron-phonon coupling exists in $M(BN)_5$ and the $T_c$ values of La(BN)$_5$ and Y(BN)$_5$ reach 69 and 59 K at ambient pressure, respectively. As a result, the high-temperature superconductivity at ambient pressure in clathrate BN compounds has been proved theoretically, which provides a way to lower the work pressure of hydride superconductors.

DOI: 10.1103/PhysRevB.106.104508

## I. INTRODUCTION

Since superconductivity was discovered by Onnes more than 100 years ago [1], exploring materials with higher superconducting transition temperature ($T_c$) has been one of the topics in condensed matter physics. Recently, great breakthroughs have been achieved in dense hydrides. Sulfur hydride was predicted to have a $T_c$ of 204 K at high pressure of 200 GPa [2]. And experiments have confirmed the superconductivity of sulfur hydride with $T_c \sim 203$ K at 155 GPa [3]. Subsequently, superconductivity close to 0 °C, $T_c \sim$ 250–260 K, was observed in lanthanum hydride at 180–170 GPa [4,5]. Moreover, superconductivity over 0 °C, $T_c \sim 287$ K, was observed in a carbonaceous sulfur hydride system at 267 GPa [6]. Most recently, superconductivity in excess of 200 K was also observed in other hydrides, such as 262 K in yttrium superhydride at 182 GPa [7], 243 K in yttrium hydride at 201 GPa [8], 224 K in $YH_6$ at 166 GPa [9], 215 K in $CaH_6$ at 172 GPa [10], 210 K in calcium superhydride at 160 GPa [11], and 253 K in lanthanum-yttrium ternary hydrides at 183 GPa [12]. These findings indicate that light-element compounds such as hydrides are potential high-temperature or room-temperature superconductors. However, a problem that cannot be ignored is that the pressure conditions required to produce such a superconducting critical temperature are very harsh. The stable pressure point is above 100 GPa or even 150 GPa for most hydrides with high-$T_c$ values. Such high-pressure conditions are hard obtain in general laboratories and also limit the potential technological applications for these high-temperature superconductors. Therefore, it is highly desired to explore light-element high-temperature superconductors at lower pressures even at ambient pressure.

There are usually two ways to reduce the phase transition pressure: one is to explore new structures, and the other is to replace elements on the existing structures. Some typical works have attracted much interest. In some metal-intercalated molecular crystals, the high-$T_c$ superconductivity below 1 megabar was predicted, such as 84 K in $MgCH_4$ with $P4/nmm$ space group at 75 GPa [13], 98 K in $Li_2BH_6$ with $Fm\bar{3}m$ space group at 100 GPa [14], 44 K in $Ba(CH_4)_3$ with $Amm2$ space group at 90 GPa [15], 146 K in $KB_2H_8$ with $Fm\bar{3}m$ space group at 12 GPa [16], 55 K in $MgC_2H_8$ at 40 GPa, and 67 K in $MgC_2H_8$ at 80 GPa with $Fm\bar{3}m$ space group [17]. In some ternary metal hydrides with clathrate structures and $Fm\bar{3}m$ space group, the transition pressure is reduced below 100 GPa and the $T_c$ is maintained at a high level. For example, $LaBH_8$ can exhibit the superconductivity of 126–156 K at 50–55 GPa [18,19]. $LaC_2H_8$ can also be superconducting at 70 GPa with $T_c = 69$ K [20]. Even $LaBeH_8$ can superconduct at 20 GPa and maintain $T_c$ close to 158 K [21], as well as the $T_c \sim 126$ K of $SrSiH_8$ at

*gh.zhong@siat.ac.cn
†cl.yang@siat.ac.cn
‡xjchen@hpstar.ac.cn

 ©2022 American Physical Society

27 GPa [22]. Additionally, in covalent nonmetallic hydrides, Cl-doped $H_3S$, $H_6SCl$, the transition pressure can be reduced below megabar and the superconductivity above 150 K can be maintained [23].

However, most of the above hydrogen-rich compounds are formed under specific conditions; maintaining stability requires a certain pressure, so these systems are difficult to exist stably at ambient pressure. Replacing hydrogen with other light elements is considered a feasible way to realize high-$T_c$ superconductivity at ambient pressure, since the ambient-pressure superconductivity was predicted in $Ca(BC)_3$ ($T_c \sim$ 48 K) [24], $Sr(BC)_3$ ($T_c \sim$ 40–44 K) [24,25], $Ba(BC)_3$ ($T_c \sim$ 43 K) [25], and $Ba_{0.5}Sr_{0.5}(BC)_3$ ($T_c \sim$ 75 K) [26], respectively. Similar to these $M(BC)_3$ ($M$ represents metal element) [24–26] where H in $CaH_6$ [27] is replaced by B and C, we also reported the superconductivity at ambient pressure by substituting B and N for H in $CaH_6$. By tuning metal, we predicted that $M(BN)_3$ with more dopants has higher $T_c$ than $M_{0.5}(BN)_3$ at ambient pressure, such as 72 K of $Al(BN)_3$ [28] comparing with 47 K of $Al_{0.5}(BN)_3$ [29]. Given the $sp^3$ bonding that forms in BN frameworks, the covalent states enhance the stability at low pressures. Different from $CaH_6$, $LaH_{10}$ is another high-temperature superconductor with cage structure, and even its $T_c$ is higher than that of $CaH_6$ [27,30]. So does the hydrogen in $LaH_{10}$ have high-temperature superconductivity at ambient pressure after being replaced by B and N? To answer this question, we have studied the stability, electronic structures, dynamic properties, and electron-phonon interactions of $La(BN)_5$ and $Y(BN)_5$ at ambient pressure based on first-principles calculations.

## II. COMPUTATIONAL DETAILS

At ambient pressure, the structural optimizations and self-consistent energy calculation were carried out by employing the Vienna *ab initio* simulation package (VASP) [31,32] based on the exchange-correlation functional of generalized gradient approximation in versions of Perdew-Burke-Ernzerhof [33] and projector augmented wave (PAW) pseudopotentials [34]. The plane-wave cutoff energy was set as 600 eV. In the optimization process, convergence thresholds were set as $10^{-5}$ eV in energy and $10^{-3}$ eV/Å in force. The $k$-point interval distribution of Monkhorst-Pack was 0.03 $Å^{-1}$ for structural optimization and 0.02 $Å^{-1}$ for self-consistent energy calculation, respectively.

By employing the QUANTUM ESPRESSO package (QE) [35,36], we calculated phonon frequencies and electron-phonon interactions of $La(BN)_5$ and $Y(BN)_5$. The cutoff energy of 80 Ry was used for wave functions. The PAW-type pseudopotentials for B, N, and La (B.pbe-n-kjpaw-psl.1.0.0.UPF, N.pbe-n-kjpaw-psl.1.0.0.UPF, and La.pbe-spfn-kjpaw-psl.1.0.0.UPF) were used in the QE code. The $k$-point grid of Monkhorst-Pack of $12\times12\times12$ was used in the phonon spectral calculations, and the double $k$-point grid was used in the calculation of the electron-phonon interaction matrix element. In both VASP and QE codes, the same functional was selected. Forces and stresses for the converged structures were optimized and checked to be within the error allowance of the VASP and QE codes. Based on the calculated Eliashberg

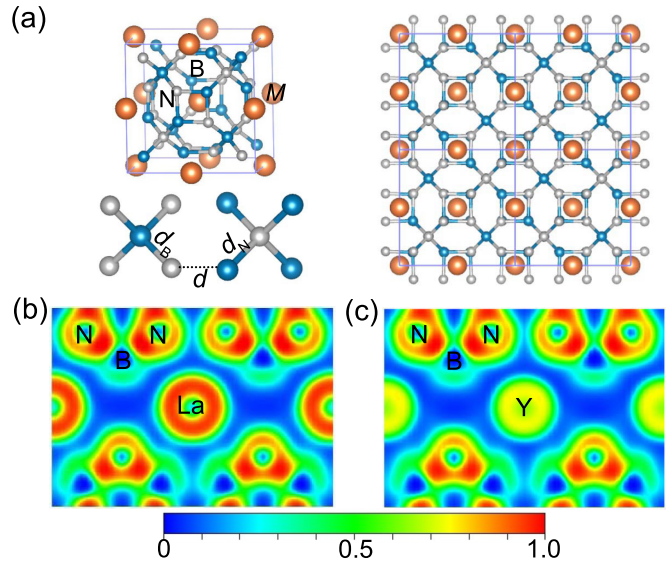


FIG. 1. (a) Crystal structure of $M(BN)_5$. (b) and (c) are corresponding to ELF on the (110) plane of $La(BN)_5$ and $Y(BN)_5$, respectively.

spectral function [$\alpha^2F(\omega)$],

$$\alpha^2F(\omega) = \frac{1}{2\pi N(0)} \sum_{Q\nu} \frac{\gamma_{Q\nu}}{\omega_{Q\nu}} \delta(\omega - \omega_{Q\nu}), \tag{1}$$

the electron-phonon coupling (EPC) constant ($\lambda$) is obtained:

$$\lambda = 2\int_0^\infty \frac{\alpha^2F(\omega)}{\omega} d\omega. \tag{2}$$

Furthermore, $T_c$ was estimated by the Allen-Dynes-corrected McMillan equation [37], expressed as

$$T_c = f_1 f_2 \frac{\omega_{\log}}{1.2} \exp\left[-\frac{1.04(1+\lambda)}{\lambda - \mu^*(1+0.62\lambda)}\right]. \tag{3}$$

In the modified McMillan equation, $\mu^\star$ represents the Coulomb pseudopotential which was taken as 0.1 in our calculations. $\omega_{\log}$ is the logarithmic average of phonon frequency,

$$\omega_{\log} = \exp\left[\frac{2}{\lambda}\int_0^\infty \frac{\alpha^2F(\omega)\log(\omega)}{\omega} d\omega)\right]. \tag{4}$$

The factor $f_1f_2$ depends on the $\lambda$, $\mu^\star$, $\omega_{\log}$, and mean-square frequency ($\overline{\omega_2}$) [37].

## III. RESULTS AND DISCUSSION

Figure 1(a) shows the crystal structural characteristics of $M(BN)_5$ ($M$ = La and Y). The symmetry of the crystal is reduced to $F\bar{4}3m$ from $Fm\bar{3}m$ when the H atoms in cage are replaced by B and N atoms. Under periodic conditions, the cages overlap and repeat in three crystal directions. Different from the clathrate structure formed by H atoms in $LaH_{10}$ [30], $(BN)_5$ cage exhibits a slight distortion due to the polar covalent bonding between B and N. The optimized crystal lattice constants of $La(BN)_5$ and $Y(BN)_5$ are $a = b = c = 7.008$ Å and $a = b = c = 6.950$ Å at ambient pressure, respectively. There are three kinds of B-N bonds in $(BN)_5$ cage: B-N bonds

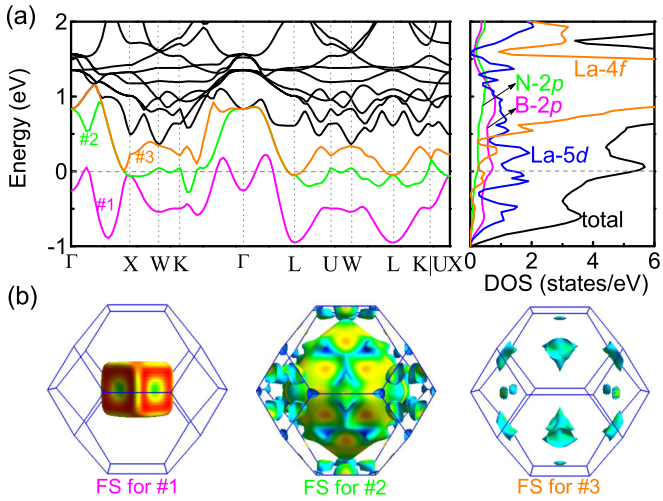


FIG. 2. (a) Calculated band structure along high-symmetry $k$-point paths of $La(BN)_5$ and total and projected DOS on atoms. Three bands crossing Fermi level are marked as #1, #2, and #3. (b) Fermi surfaces corresponding to #1, #2, and #3 bands crossing Fermi level, respectively.

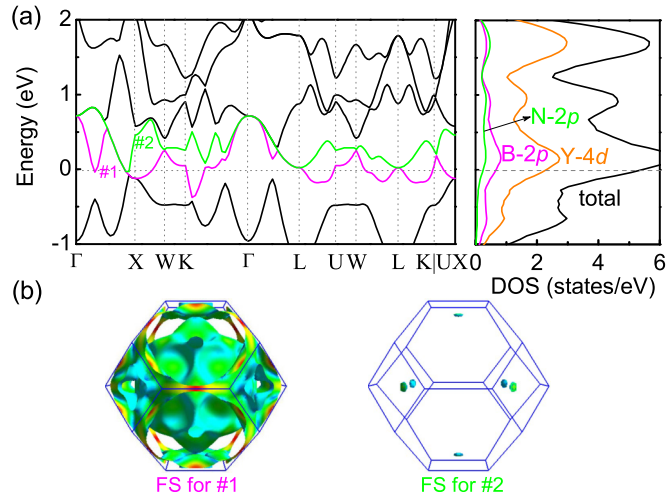


FIG. 3. (a) Calculated band structure along high-symmetry $k$-point paths of $Y(BN)_5$ and total and projected DOS on atoms. Two bands crossing Fermi level are marked as #1 and #2. (b) Fermi surfaces corresponding to #1 and #2 bands crossing Fermi level, respectively.

with B as tetrahedral center ($d_B$), B-N bonds with N as tetrahedral center ($d_N$), and B-N bonds linking two tetrahedrons ($d$). For the undoped case, these three bond lengths of $d_B$, $d_N$, and $d$ are 1.519, 1.612, and 1.582 Å, respectively. When La doping, $La(BN)_5$, these three bond lengths increase to 1.570, 1.650, and 1.646 Å, respectively. For $Y(BN)_5$, they are 1.555, 1.636, and 1.634 Å, respectively. La has a greater influence on the B-N bonds than Y. The electron localization functions (ELFs) shown in Figs. 1(b) and 1(c) depict the bonding feature in $M(BN)_5$. The polar covalent bonding forms between B and N with $sp^3$ hybridization, which is the main reason that $M(BN)_5$ can be stabilized at ambient pressure. Metal La and Y exist in the form of ionic bonding. Based on the Bader charge calculation [38,39], the charge transferred from $M$ to $(BN)_5$ cage is 1.15$e$ per La for $La(BN)_5$ and 1.30$e$ per Y for $Y(BN)_5$, respectively. The charge transfer in $M(BN)_5$ is stronger than that in $MH_{10}$ [40]. The strong anion-cation interaction increases the Madelung energy of the ionic component of the $M$-$BN_5$ bonding, which also increases the stability of $M(BN)_5$.

$(BN)_5$ clathrate crystal without doping metal is an insulator with a band gap of 4.13 eV. However, when the metal doped into $(BN)_5$ cage, the Fermi level shifts toward a higher energy level because of the existence of charge transfer from metal to $(BN)_5$ sublattice. The metallization of $La(BN)_5$ and $Y(BN)_5$ is demonstrated by electronic structures shown in Figs. 2 and 3, respectively. For $La(BN)_5$, there are three half-filled bands crossing the Fermi level in Fig. 2(a), correspondingly forming the electron- and holelike Fermi surfaces (FSs). As shown in Fig. 2(b), band #1 forms the typical holelike FS sheets while bands #2 and #3 form the complicated near-electronlike FS sheets. The electronic density of states (DOS) projected on atomic orbitals indicate that the electronic states near the Fermi level mainly come from La 5$d$, La 4$f$, B 2$p$, and N 2$p$ electrons. However, the contribution of La 5$d$ electrons to the DOS values at Fermi level [$N(E_F)$] is obviously the largest in $La(BN)_5$, which is different from $LaH_{10}$ at 250 GPa where the contribution of H $s$ electrons to $N(E_F)$ is larger than that of La, and even the contribution of La 4$f$ is larger than that of La 5$d$ [30]. The $N(E_F)$ for $La(BN)_5$ is about 1.25 states/eV/f.u., which is obviously larger than 0.74 states/eV/f.u. of $LaH_{10}$ at 250 GPa [30]. For $Y(BN)_5$, only two bands cross the Fermi level. As shown in Figs. 3(a) and 3(b), band #1 leads to a complicated FS sheet containing electron and hole characteristics while band #2 results in the electronlike FS sheets. Every element contributes to the electronic states near Fermi level, but Y 4$d$ contributes the most similar to that in $La(BN)_5$. The $N(E_F)$ for $Y(BN)_5$ is about 1.33 states/eV/f.u., which is also larger than 0.88 states/eV/f.u. of $YH_{10}$ at 250 GPa [30]. For phonon-mediated superconductors, the bigger $N(E_F)$ values implies the stronger superconductivity in $M(BN)_5$.

To examine the possible high-$T_c$ superconductivity, we investigated phonon characteristics and electron-phonon coupling (EPC) interactions of $La(BN)_5$ and $Y(BN)_5$. Figure 4 presents the phonon spectra along high-symmetry $k$-point paths, projected phonon density of states (PhDOS) on element, Eliashberg spectrum function $\alpha^2F(\omega)$, and EPC integral $\lambda(\omega)$. As shown in Figs. 4(a) and 4(d), the absence of imaginary frequencies in phonon spectra indicates that both $La(BN)_5$ and $Y(BN)_5$ are dynamically stable at ambient pressure. Comparing with hydrides, the phonon frequencies of boron-nitrogen compounds are visibly lower; less than 1200 $cm^{-1}$ in $La(BN)_5$ and $Y(BN)_5$. Combining with the PhDOS shown in Figs. 4(b) and 4(e), the metal atoms mainly contribute to phonon modes in the low-frequency regions below 320 $cm^{-1}$ for La and below 150 $cm^{-1}$ for Y. In addition, the B and N atoms dominate the vibrational modes in the frequency ranges of 100–1050 $cm^{-1}$ of $La(BN)_5$ and 150–1130 $cm^{-1}$ of $Y(BN)_5$. However, the PhDOS indicates that vibrations of B and N atoms above 1000 $cm^{-1}$ are very weak. Based on the bonding analysis above, we can identify that at around 900 $cm^{-1}$ for $La(BN)_5$ and 950 $cm^{-1}$ for $Y(BN)_5$, the modes

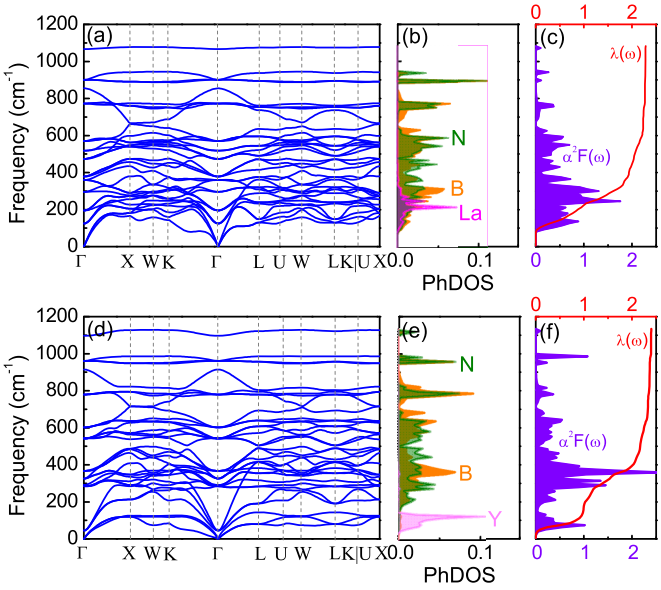


FIG. 4. Calculated phonon spectra along high-symmetry $k$-point paths, projected PhDOS on element, Eliashberg spectrum function $\alpha^2F(\omega)$, and EPC integral $\lambda(\omega)$. (a)–(c) correspond to $La(BN)_5$, while (d)–(f) correspond to $Y(BN)_5$.

are mainly induced by B-N stretching vibrations in $BN_4$ unit, while around 760 cm$^{-1}$ for $La(BN)_5$ and 780 cm$^{-1}$ for $Y(BN)_5$, the modes are owing to B-N stretching vibrations in $NB_4$ unit and the linking vibrations between $BN_4$ and $NB_4$ units. The phonon modes in the middle-frequency region of 100–600 cm$^{-1}$ for $La(BN)_5$ and 150–650 cm$^{-1}$ for $Y(BN)_5$ originate B-N bending vibrations and the coupling among $(BN)_5$ cages. The EPC interactions were explored by calculating the Eliashberg spectral function $\alpha^2F(\omega)$. The total EPC constant $\lambda$ is obtained by the EPC integral shown in Figs. 4(c) and 4(f). Then, based on the $\lambda$ and the logarithmic average of phonon frequency $\omega_{\log}$, the superconducting transition temperature $T_c$ was further estimated by using Eq. (3). The superconducting parameters are summarized in Table I. The total $\lambda$ at ambient pressure is 2.28 for $La(BN)_5$ and 2.39 for $Y(BN)_5$, respectively, which is comparable with those of $LaH_{10}$ and $YH_{10}$ as shown in Table I. In $La(BN)_5$, the contribution of La (by charge transfer) to total $\lambda$ is about 45.9%, and the contribution of $(BN)_5$ cage is about 54.1%. In $Y(BN)_5$, the contribution of Y (by charge transfer) to total $\lambda$ is about 41.2%, and the contribution of $(BN)_5$ cage is about 58.8%. Thus, the phonon vibration of the La or Y atom has an important influence on the EPC constant of $M(BN)_5$. However, in $LaH_{10}$, the La atom only contributes to 12% of the total EPC constant [41]. When $\mu^\star = 0.1$, the $T_c$ is predicted as 69.2 K for $La(BN)_5$ and 59.1 K for $Y(BN)_5$ at ambient pressure, respectively. It is found that the parameter of Coulomb pseudopotential has little effect on $T_c$ as shown in Table I. As a comparison, for $(BN)_3$ cages with $CaH_6$-like structure, Y doping [$Y(BN)_3$] is unstable at considered pressures, while La doping [$La(BN)_3$] is only stable above 170 GPa [28]. In sharp contrast, La and Y dopings in $(BN)_5$ cage can be stabilized at ambient pressure and realize the superconducting transition $T_c$ near 70 or 60 K, respectively. The distinction in stability and superconductivity between doped $(BN)_5$ and $(BN)_3$ clathrates is mainly due to the difference of structures after doping. The B-N bond lengths are 1.707 and 1.694 Å in La-doped and Y-doped $(BN)_3$ clathrates, respectively. However, in La-doped and Y-doped $(BN)_5$ cages, the B-N bond lengths are shortened to the ranges of 1.570–1.650 and 1.555–1.636 Å, respectively. The strong interaction caused by the change of B-N bond length may be the key for $M(BN)_5$ to stabilize and exhibit high-temperature superconductivity at ambient pressure.

As a result, both $La(BN)_5$ and $Y(BN)_5$ with structural characteristics similar to $LaH_{10}$ are suggested to be superconducting at ambient pressure with $T_c$ of 69.2 and 59.1 K, respectively. The superconducting critical temperature is close to the liquid nitrogen temperature region. Unfortunately, these $T_c$ values are still lower than those of hydrides. This situation is not consistent with the higher $N(E_F)$ and the comparable EPC constant in $M(BN)_5$ with $MH_{10}$. Analyzing the superconducting parameters in Table I, we can find that the main reason for the $T_c$ of BN compounds being lower than that of hydrides is that BN compounds have much lower $\omega_{\log}$ values. And this $\omega_{\log}$ value is related to the compactness (or pressure) of the material. In the pursuit of low-pressure and high-$T_c$ superconductivity, it seems to be a contradiction. However, with $M(BN)_5$ as a preliminary test, the feasibility of high-temperature superconductivity at ambient pressure has been explored. We predict that the $\omega_{\log}$ value can be increased through further chemical precompression such as changing the type and concentration of dopants, so as to further improve $T_c$ at ambient pressure or at low pressures. Finally, the thermodynamical stability has been examined to analyze the possibility of experimental synthesis of $La(BN)_5$ and $Y(BN)_5$. The enthalpy of formation was calculated at ambient pressure by assuming several possible decomposition paths such as element phases [42], binary borides [42], nitrides [42],

TABLE I. Superconducting parameters of $La(BN)_5$ and $Y(BN)_5$ at ambient pressure.

| System | Pressure (GPa) | $\lambda$ | $\omega_{\log}$ (K) | $N(E_F)$ (states/eV/f.u.) | $T_c$ (K, $\mu = 0.13$) | $T_c$ (K, $\mu = 0.1$) |
|---|---|---|---|---|---|---|
| $La(BN)_5$ | 0 | 2.28 | 335.3 | 1.25 | 63.0 | 69.2 |
| $Y(BN)_5$ | 0 | 2.39 | 270.2 | 1.33 | 55.7 | 59.1 |
| $LaH_{10}$[a] | 250 | 2.29 | 1253 | 0.74 | 257 | 274 |
| $YH_{10}$[b] | 250 | 2.58 | 1282 | 0.88 | 305 | 326 |

[a]Ref.[30].
[b]Ref. [30]

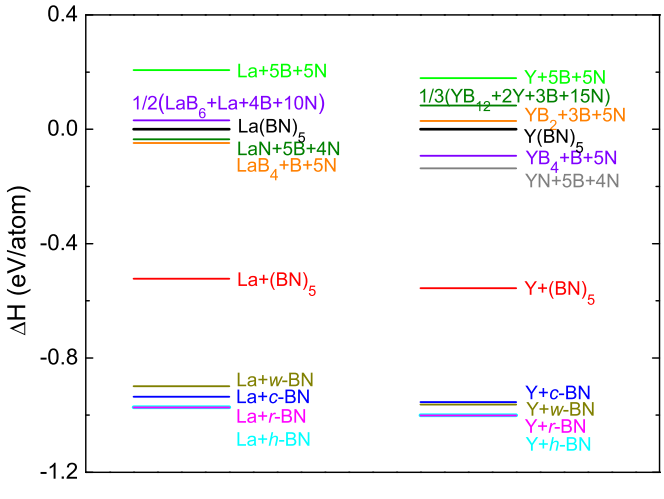


FIG. 5. Calculated possible decomposition enthalpies relative to the enthalpy of $M(BN)_5$ ($M$ = La and Y).

and boron nitrides ($c$-BN [29,43,44], $h$-BN [29,43,45], $r$-BN [29,43,46], and $w$-BN [29,43,47]). The zero-point energy effect has also been taken into account in the calculation of enthalpies. Figure 5 shows the enthalpy difference between $M(BN)_5$ and decomposition products, referenced to the enthalpy of $M(BN)_5$. The result indicates that both $La(BN)_5$ and $Y(BN)_5$ are thermodynamically metastable. The maximum of enthalpy difference between $M(BN)_5$ and $M + BN$ compounds is about 0.9 eV/atom. However, this does not completely rule out the possibility of experimental synthesis of this predicted $M(BN)_5$ with the clathrate structure. Some clathrate structures with high formation energy have been reported to be successfully experimentally synthesized. For example, the calculated formation energy of clathrate $I_{9.5}Si_{44.5}$ is above convex hull 0.13 eV/atom [48], and the calculated formation energy of $SiB_6$ and $C_{60}$ could reach 0.289 eV/atom [49] and 0.350 eV/atom [50], but all compounds mentioned above have been successfully synthesized [51–53]. Encouragingly, the enthalpy of $La(BN)_5$ is less than those of La + B + N and $1/2(LaB_6 + La + 4B + 10\ N)$, while the enthalpy of $Y(BN)_5$ is less than those of Y + B + N, $1/3(YB_{12} + 2Y + 3B + 15N)$, and $YB_2 + 3B + 5N$, respectively. These results suggest that these two materials can be synthesized for these special reaction routes under certain conditions.

## IV. CONCLUSION

In summary, in order to explore the high-temperature superconductivity at ambient pressure, we have constructed a $(BN)_5$ clathrate structure with B and N elements by mimicking the H cage structure in $LaH_{10}$, and then doped with metals La and Y to observe the crystal characteristics, electronic structures, dynamic properties, and electron-phonon interactions within the framework of the first principles. With the help of charge transfer from metal to $(BN)_5$ cage, $La(BN)_5$ and $Y(BN)_5$ exhibit good metallic features at ambient pressure. The strong $sp^3$ hybridization between B and N atoms drives the stability of $M(BN)_5$ at lower pressure compared with $MH_{10}$. The phonon spectra also confirm that $M(BN)_5$ is dynamically stable at ambient pressure. Although the phonon frequencies are greatly reduced after B and N replace H, the EPC constant $\lambda$ remains at an order of magnitude comparable to $MH_{10}$, such as 2.28 for $La(BN)_5$ and 2.39 for $Y(BN)_5$. $T_c$ is predicted to be 69.2 K for $La(BN)_5$ and 59.1 K for $Y(BN)_5$, respectively. The low $\omega_{log}$ value causes the $T_c$ of $M(BN)_5$ to be lower than those of $LaH_{10}$ and $YH_{10}$ at 250 GPa. However, we have revealed the feasibility of high-temperature superconductivity at ambient pressure of BN compounds with $LaH_{10}$-like structure. Furthermore, we infer that the $T_c$ of clathrate BN compounds can be improved by changing dopants.

## ACKNOWLEDGMENTS

This work was supported by the National Natural Science Foundation of China (Grant No. 12074401) and the Shenzhen Science and Technology Program (Grants No. JCYJ20180507182445460, No. JCYJ20200109112810241, and No. KQTD20200820113045081). This work was also supported by the SIAT-CUHK Joint Laboratory of Photovoltaic Solar Energy. The calculations were performed in HPC Lab, National Supercomputing Center in Shenzhen.

[1] H. K. Onnes, in *Through Measurement to Knowledge. Boston Studies in the Philosophy of Science*, edited by K. Gavroglu and Y. Goudaroulis (Springer, Dordrecht, 1991).

[2] D. Duan, Y. Liu, F. Tian, D. Li, X. Huang, Z. Zhao, H. Yu, B. Liu, W. Tian, and T. Cui, Sci. Rep. **4**, 6968 (2015).

[3] A. P. Drozdov, M. I. Eremets, I. A. Troyan, V. Ksenofontov, and S. I. Shylin, Nature (London) **525**, 73 (2015).

[4] A. P. Drozdov, P. P. Kong, V. S. Minkov, S. P. Besedin, M. A. Kuzovnikov, S. Mozaffari, L. Balicas, F. F. Balakirev, D. E. Graf, V. B. Prakapenka, E. Greenberg, D. A. Knyazev, M. Tkacz, and M. I. Eremets, Nature (London) **569**, 528 (2019).

[5] M. Somayazulu, M. Ahart, A. K. Mishra, Z. M. Geballe, M. Baldini, Y. Meng, V. V. Struzhkin, and R. J. Hemley, Phys. Rev. Lett. **122**, 027001 (2019).

[6] E. Snider, N. Dasenbrock-Gammon, R. McBride, M. Debessai, H. Vindana, K. Vencatasamy, K. V. Lawler, A. Salamat, and R. P. Dias, Nature (London) **586**, 373 (2020).

[7] E. Snider, N. Dasenbrock-Gammon, R. McBride, X. Wang, N. Meyers, K. V. Lawler, E. Zurek, A. Salamat, and R. P. Dias, Phys. Rev. Lett. **126**, 117003 (2021).

[8] P. Kong, V. S. Minkov, M. A. Kuzovnikov, A. P. Drozdov, S. P. Besedin, S. Mozaffari, L. Balicas, F. F. Balakirev, V. B. Prakapenka, S. Chariton, D. A. Knyazev, E. Greenberg, and M. I. Eremets, Nat. Commun. **12**, 5075 (2021).

[9] I. A. Troyan, D. V. Semenok, A. G. Kvashnin, A. V. Sadakov, O. A. Sobolevskiy, V. M. Pudalov, A. G. Ivanova, V. B. Prakapenka, E. Greenberg, A. G. Gavriliuk, I. S. Lyubutin, V. V. Struzhkin, A. Bergara, I. Errea, R. Bianco, M. Calandra, F.

Mauri, L. Monacelli, R. Akashi, and A. R. Oganov, Adv. Mater. **33**, 2006832 (2021).
[10] L. Ma, K. Wang, Y. Xie, X. Yang, Y. Wang, M. Zhou, H. Liu, X. Yu, Y. Zhao, H. Wang, G. Liu, and Y. Ma, Phys. Rev. Lett. **128**, 167001 (2022).
[11] Z. Li, X. He, C. Zhang, X. Wang, S. Zhang, Y. Jia, S. Feng, K. Lu, J. Zhao, J. Zhang, B. Min, Y. Long, R. Yu, L. Wang, M. Ye, Z. Zhang, V. Prakapenka, S. Chariton, P. A. Ginsberg, J. Bass *et al.*, Nat. Commun. **13**, 2863 (2022).
[12] D. V. Semenok, I. A. Troyan, A. G. Ivanova, A. G. Kvashnin, I. A. Kruglov, M. Hanfland, A. V. Sadakov, O. A. Sobolevskiy, K. S. Pervakov, I. S. Lyubutin, K. V. Glazyrin, N. Giordano, D. N. Karimov, A. L. Vasiliev, R. Akashi, V. M. Pudalov, and A. R. Oganov, Mater. Today **48**, 18 (2021).
[13] F. Tian, D. Li, D. Duan, X. Sha, Y. Liu, T. Yang, B. Liu, and T. Cui, Mater. Res. Express **2**, 046001 (2015).
[14] C. Kokail, W. von der Linden, and L. Boeri, Phys. Rev. Materials **1**, 074803 (2017).
[15] M.-J. Jiang, H.-L. Tian, Y.-L. Hai, N. Lu, P.-F. Tong, S.-Y. Wu, W.-J. Li, C.-L. Yang, and G.-H. Zhong, ACS Appl. Electron. Mater. **3**, 4172 (2021).
[16] M. Gao, X.-W. Yan, Z.-Y. Lu, and T. Xiang, Phys. Rev. B **104**, L100504 (2021).
[17] M.-J. Jiang, Y.-L. Hai, H.-L. Tian, H.-B. Ding, Y.-J. Feng, C.-L. Yang, X.-J. Chen, and G.-H. Zhong, Phys. Rev. B **105**, 104511 (2022).
[18] S. Di Cataldo, C. Heil, W. von der Linden, and L. Boeri, Phys. Rev. B **104**, L020511 (2021).
[19] X. Liang, A. Bergara, X. Wei, X. Song, L. Wang, R. Sun, H. Liu, R. J. Hemley, L. Wang, G. Gao, and Y. Tian, Phys. Rev. B **104**, 134501 (2021).
[20] A. P. Durajski and R. Szczesniak, Phys. Chem. Chem. Phys. **23**, 25070 (2021).
[21] Z. Zhang, T. Cui, M. J. Hutcheon, A. M. Shipley, H. Song, M. Du, V. Z. Kresin, D. Duan, C. J. Pickard, and Y. Yao, Phys. Rev. Lett. **128**, 047001 (2022).
[22] R. Lucrezi, S. Di Cataldo, W. von der Linden, L. Boeri, and C. Heil, npj Comput. Mater. **8**, 119 (2022).
[23] Y.-L. Hai, H.-L. Tian, M.-J. Jiang, H.-B. Ding, Y.-J. Feng, G.-H. Zhong, C.-L. Yang, X.-J. Chen, and H.-Q. Lin, Phys. Rev. B **105**, L180508 (2022).
[24] S. Di Cataldo, S. Qulaghasi, G. B. Bachelet, and L. Boeri, Phys. Rev. B **105**, 064516 (2022).
[25] J.-N. Wang, X.-W. Yan, and M. Gao, Phys. Rev. B **103**, 144515 (2021)
[26] P. Zhang, X. Li, X. Yang, H. Wang, Y. Yao, and H. Liu, Phys. Rev. B **105**, 094503 (2022).
[27] H. Wang, J. S. Tse, K. Tanaka, T. Iitaka, and Y. Ma, Proc. Natl. Acad. Sci. USA **109**, 6463 (2012).
[28] Y.-L. Hai, H.-L. Tian, M.-J. Jiang, W.-J. Li, G.-H. Zhong, C.-L. Yang, X.-J. Chen, and H.-Q. Lin, Mater. Today Phys. **25**, 100699 (2022).
[29] X. Li, X. Yong, M. Wu, S. Lu, H. Liu, S. Meng, J. S. Tse, and Y. Li, J. Phys. Chem. Lett. **10**, 2554 (2019).
[30] H. Liu, I. I. Naumov, R. Hoffmann, N. W. Ashcroft, and R. J. Hemley, Proc. Natl. Acad. Sci. USA **114**, 6990 (2017).
[31] G. Kresse and J. Furthmuller, Comput. Mater. Sci. **6**, 15 (1996).
[32] G. Kresse and J. Furthmuller, Phys. Rev. B **54**, 11169 (1996).
[33] J. P. Perdew, K. Burke, and M. Ernzerhof, Phys. Rev. Lett. **77**, 3865 (1996).
[34] G. Kresse and D. Joubert, Phys. Rev. B **59**, 1758 (1999).
[35] P. Giannozzi, S. Baroni, N. Bonini, M. Calandra, R. Car, C. Cavazzoni, D. Ceresoli, G. L. Chiarotti, M. Cococcioni, I. Dabo, A. Dal Corso, S. Fabris, G. Fratesi, S. de Gironcoli, R. Gebauer, U. Gerstmann, C. Gougoussis, A. Kokalj, M. Lazzeri, L. Martin-Samos *et al.*, J. Phys.: Condens. Matter **21**, 395502 (2009).
[36] P. Giannozzi, O. Andreussi, T. Brumme, O. Bunau, M. B. Nardelli, M. Calandra, R. Car, C. Cavazzoni, D. Ceresoli, M. Cococcioni, N. Colonna, I. Carnimeo, A. Dal Corso, S. de Gironcoli, P. Delugas, R. A. DiStasio, Jr., A. Ferretti, A. Floris, G. Fratesi, G. Fugallo *et al.*, J. Phys.: Condens. Matter **29**, 465901 (2017).
[37] P. B. Allen and R. C. Dynes, Phys. Rev. B **12**, 905 (1975).
[38] G. Henkelman, A. Arnaldsson, and H. Jónsson, Comput. Mater. Sci. **36**, 354 (2006).
[39] M. Yu and D. R. Trinkle, J. Chem. Phys. **134**, 064111 (2011).
[40] F. Peng, Y. Sun, C. J. Pickard, R. J. Needs, Q. Wu, and Y. Ma, Phys. Rev. Lett. **119**, 107001 (2017).
[41] C. Wang, S. Yi, and J.-H. Cho, Phys. Rev. B **100**, 060502(R) (2019).
[42] The crystal structures of element substance including dopants B and N are taken from Materials Project. https://materialsproject.org/.
[43] Y. Li, J. Hao, H. Liu, S. Lu, and J. S. Tse, Phys. Rev. Lett. **115**, 105502 (2015).
[44] P. B. Mirkarimi, K. F. McCarty, and D. L. Medlin, Mater. Sci. Eng. R **21**, 47 (1997).
[45] F. P. Bundy and J. S. Kasper, J. Chem. Phys. **46**, 3437 (1967).
[46] R. T. Paine and C. K. Narula, Chem. Rev. **90**, 73 (1990).
[47] T. Sato, T. Ishii, and N. Setaka, J. Am. Ceram. Soc. **65**, c162 (1982).
[48] T. F. Cerqueira, S. Pailhes, R. Debord, V. M. Giordano, R. Viennois, J. Shi, S. Botti, and M. A. Marques, Chem. Mater. **28**, 3711 (2016).
[49] Z. Yuan, M. Xiong, and D. Yu, Phys. Lett. A **384**, 126075 (2020).
[50] J. T. Wang, H. Weng, S. Nie, Z. Fang, Y. Kawazoe, and C. Chen, Phys. Rev. Lett. **116**, 195501 (2016).
[51] E. Reny, S. Yamanaka, C. Cros, and M. Pouchard, Chem. Commun. **24**, 2505 (2000).
[52] M. Vlasse, G. Slack, M. Garbauskas, J. Kasper, and J. Viala, J. Solid State Chem. **63**, 31 (1986).
[53] H. W. Kroto, J. R. Heath, S. C. O'Brien, R. F. Curl, and R. E. Smalley, Nature (London) **318**, 162 (1985).